Development of an MHD-Augmented, High Enthalpy, Shock Tunnel Facility

S. R. PATE,* L. G. SILER,† D. W. STALLINGS,† AND D. A. WAGNER†
ARO, Inc., Arnold Air Force Station, Tenn.

Experimental and theoretical studies conducted in support of the development of a high performance, hypersonic/hypervelocity shock tunnel facility (AEDC-VKF Tunnel J) capable of providing thermochemical equilibrium and nonequilibrium flow conditions at high enthalpies are presented. Demonstrated capabilities of the facility with and without magnetohydrodynamic (MHD) flow augmentation are shown. Increases in the flow velocity from 12,000 to 21,000 fps were obtained using an MHD nozzle accelerator with the flow seeded with potassium carbonate. Good agreement is shown to exist between one-dimensional MHD theory and experimental data for two calibrated conditions. Calibration and analysis of the flow in the MHD accelerator channel and in a two-stage nozzle system, with and without MHD augmentation, are included. It is shown that quantitative aerodynamic measurements can be obtained in an MHD-augmented shock tunnel facility. A full-scale, impulse-heated, high performance driver ($p_4 = 44{,}000$ psi, $T_4 = 800°$K) using helium and nitrogen was developed (concurrently but not in conjunction with the MHD shock tunnel) and experimental shock tube data are presented. Projected capabilities of the facility using the high performance driver are included.

Nomenclature

A_T = diaphragm opening area
B = magnetic field strength, webers/m^2
$\bar{d}$ = effective test section diameter ($\bar{d} = 0.8$ test section diameter)
H = enthalpy
h = MHD accelerator channel height
J = current density
l = driver or driven tube length
M = Mach number
M_s = shock wave Mach number
M_{s_i} = initial shock wave Mach number ($l_1 = 0$)
p = pressure
p_o' = pitot probe pressure
ρ = density
Re_∞/ft = freestream Reynolds number per foot, $\rho_\infty U_\infty/\mu_\infty$
$Re_{\infty,\bar{d}}$ = length Reynolds number based on effective test section diameter
T = temperature
t = time
$\bar{U}$ = mean flow velocity
$U_{\lim}$ = limiting velocity [$U_{\lim} = (2H_o)^{1/2}$ for inviscid, isentropic flow] [$U_{\lim} = (2H + U^2)^{1/2}$ viscous flow evaluated using conditions at exit of first-stage nozzle]
V = electrode voltage
V_F = flow-induced voltage ($V_F = \bar{U}Bh$)
x = axial distance from throat of first-stage nozzle or axial distance from inlet of second-stage nozzle
x_1 = axial distance from driver diaphragm section
y = vertical height
γ = ratio of specific heats
γ_E = isentropic exponent ($p/\rho^{\gamma_E} = \text{const}$)
μ_∞ = freestream absolute viscosity

Subscripts

1 = driven tube
4 = driver
5 = reflected wave (reservoir) conditions
1–11 = electrode number
i = second-stage nozzle inlet
o = reservoir conditions
∞ = freestream

Received October 13, 1972; revision received October 10, 1973. The research reported herein was conducted by the Arnold Engineering Development Center, Air Force Systems Command. Research results were obtained by personnel of ARO, Inc., contract operator at AEDC.

Index categories: Nozzle and Channel Flow; Plasma Dynamics and MHD; Research Facilities and Instrumentation.

* Supervisor, Impulse Tunnels and Dynamics Section, Aerodynamics Projects Branch, von Kármán Gas Dynamics Facility. Associate Fellow AIAA.

† Project Engineer, Aerodynamics Projects Branch, von Kármán Gas Dynamics Facility.

1. Introduction

A REAL-GAS, high-density, true velocity, hypersonic wind tunnel is currently needed since a significant portion of the flight envelope for the space transportation system (STS) orbiter as well as other advanced re-entry configurations will occur in a thermochemical equilibrium and nonequilibrium aerodynamic environment that cannot presently be duplicated or adequately simulated in existing ground test facilities.

Considerable attention has been devoted to applying the magnetohydrodynamic (MHD) technique for providing true velocity flows in hypersonic test facilities.[1-5] Ring[1] evaluated the potential of an MHD nozzle accelerator for producing chemical equilibrium and nonequilibrium hypersonic test conditions. He identified the Faraday-type (J × B) accelerator driven by an impulse facility as offering the best performance potential for obtaining flow velocities near 25K fps at high-density levels. Ring also concluded that if a highly disassociated nozzle freestream flow was to be prevented, a seed material would be necessary to provide the required electrical conductivity.

Norman[2] analytically studied the performance of a J × B segmented accelerator with optimum flow velocity when operated with a constant static temperature, constant loading factor and using $\frac{1}{4}\%$ of potassium seed for various inlet pressures and temperatures. The equations for one-dimensional MHD flow, considering both ideal- and nonideal-gas effects, have also been published by Norman.[3]

Preliminary experimental performance results obtained in an MHD-augmented shock tunnel have been reported by Warren, Harris et al.[4] A limited amount of experimental performance data has been obtained in a hotshot facility driving a Faraday-type MHD nozzle accelerator, and flow velocity increases from 16K fps to 24K fps were obtained in a nitrogen test gas seeded with potassium, as reported by Grabowsky, Durran, and Mirels.[5] To the authors' knowledge, no aerodynamic data obtained in an MHD-augmented facility have been published.

Leonard and Rose[6] identified the need for specific hypersonic, high Reynolds number, high enthalpy equilibrium and nonequilibrium test conditions not presently achievable in existing

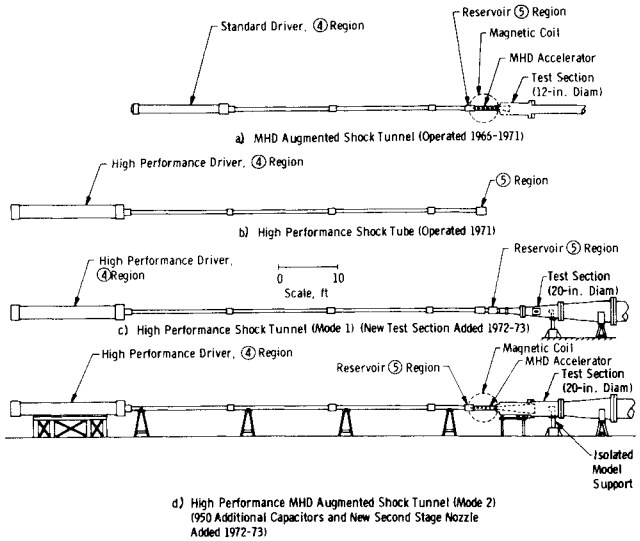

Fig. 1 Tunnel J configurations.

facilities. They evaluated high performance facility concepts and studied the feasibility of a single impulse facility which would have equilibrium expansion in the nozzle. They concluded that a shock tunnel driving a Faraday ($J \times B$) magnetohydrodynamic (MHD) segmented accelerator was one of three concepts offering the most promise.

A review and critique of high performance, shock tunnel driving techniques has been presented recently by Warren and Harris.[7]

This paper describes the facility hardware and the demonstrated and projected capabilities of the AEDC-VKF Tunnel J shock tunnel facility with and without MHD flow augmentation (Fig. 1).‡ The facility components that were used in obtaining the experimental data presented in this paper are illustrated in Figs. 1a and 1b. A full-scale, high performance shock tunnel driver was developed concurrently with the MHD nozzle accelerator. The recently modified Tunnel J facility as now exists, but which has not yet been operated, is illustrated in Figs. 1c and 1d. A summary of the achieved and predicted capabilities is included in Table 1. Additional information has been published in Ref. 8.

2. Description of Equipment

2.1 Shock Tunnel Drivers and Driven Tube

The standard driver has a 3.5-in.-internal-diam and is approximately 15 ft in length, as illustrated in Fig. 1a. The driver gas (usually helium or hydrogen) is heated to temperatures up to 550°K by external resistance heating elements attached to the driver. When hydrogen is used, the effective internal driver length is reduced to about 5 ft because of safety requirements. Routine operation is currently conducted over a driver pressure range from about 5000 psi to a maximum of about 15,000 psi using a stainless steel single-diaphragm system. All MHD operation to date has utilized this driver.

The full-scale high performance driver§ is illustrated in Fig. 1. The internal structure of this impulse-heated, high performance driver is very complex since many intricate components comprise the driver system. The driver consists of four major components: 1) a pressure vessel about 21 ft long with a 27-in.-outside-diam and an 11-in.-diam internal bore; 2) a 10.5-in.-external-diam by 17-ft-in-length internal electrical-thermal

‡ Initial direction and original concepts were by J. D. Whitfield, W. S. Norman, and G. D. Norfleet of ARO, Inc.

§ R. L. Watkins Jr. was the engineer primarily responsible for the development of this driver.

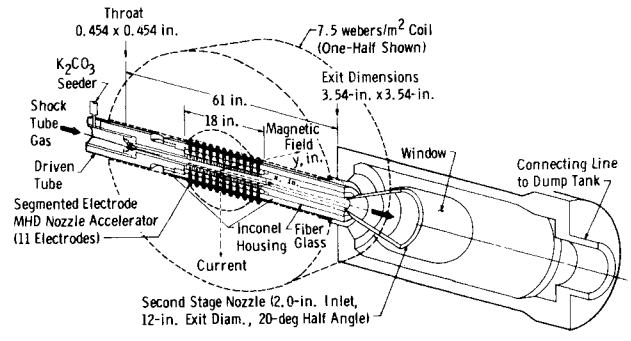

Fig. 2 Schematic of the MHD accelerator, magnetic coil and interim second-stage nozzle.

insulator vessel; 3) a 7-in.-internal-diam by 15-ft-in-length eccentric, stainless steel heater element supported by 150 small Alumina® electrical insulator blocks; and 4) a double-diaphragm section with each diaphragm rated for about 34,000 psi. The pressure vessel has been hydrostatically tested to its design pressure of 100,000 psia. The stainless steel eccentric heater element is designed for 1600°F (1145°K) and a driver gas pressure of 50,000 psi. The present double-diaphragm section is designed for a 50,000-psi total pressure load. Helium and nitrogen, or a mixture of these two gases, are used as the driver gases. Hydrogen will not be used as a driver gas with Tunnel J in its present location because of safety restrictions.

Driven tube lengths of 45 ft and 63 ft are used with the standard driver ($l_1/d_1 = 135$) and the high performance driver ($l_1/d_1 = 189$), respectively. Each tube section has an inside diameter of 4 in. and an outside diameter of 8.5 in. Up to twenty ports are available for measuring shock tube pressures and shock wave velocities.

2.2 Nozzles and MHD Accelerator

Sketches illustrating the MHD accelerator first-stage nozzle

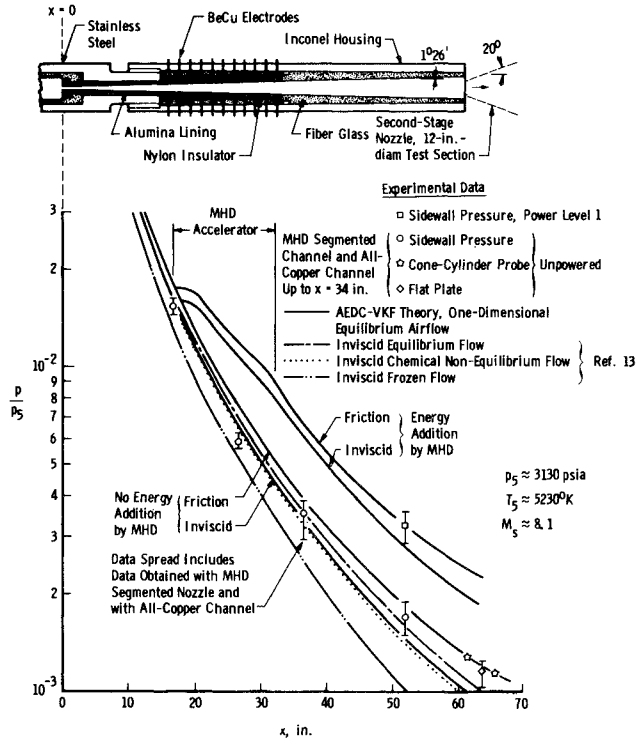

Fig. 3 Static pressure distributions in first-stage nozzle, with and without MHD augmentation.

Table 1 Tunnel J—performance capabilities

CONFIG.	DRIVER ④REGION	RESERVOIR ⑤ REGION	MAGNETIC COIL	MHD ACCELERATOR	TEST SECTION
MHD Facility Fig. 1A (Achieved)	p_4 = 14,500 psia T_4 = 500°K Hydrogen Gas	$p_5 \approx$ 3500 psia $T_5 \approx$ 5000°K $M_S \approx$ 8.0 (Tailored Interface)	0	$\bar{U}_1$ = 9,700 fps $\bar{M}_1$ = 2.9 $\bar{U}_{11}$ = 10,300 fps $\bar{M}_{11}$ = 3.4 M_i = 3.95	Density, h = 164,000 ft M_∞ = 10 U_∞ = 12,000 fps U_{lim} = 12,600 fps $H_0 = 8 \times 10^7$ ft^2/sec^2 s/r = 31.8 Re_∞/ft = 0.070 x 10^6
			4w/m^2	$\bar{U}_{11}$ = 15,300 fps $\bar{M}_{11}$ = 3.9 M_i = 4.3	Density, h = 165,000 ft M_∞ = 10 U_∞ = 17,000 U_{lim} = 19,000 fps Stagnation Enthalpy = 1.8 x 10^8 ft^2/sec^2 s/r = 36.0 Re_∞/ft = 0.05 x 10^6
			5w/m^2 Mass Fraction of Seed ≈ 1%	$\bar{U}_{11}$ = 19,100 fps $\bar{M}_{11}$ = 4.7 M_i = 5.1	Density, h = 153,000 ft M_∞ = 10 U_∞ = 21,000 fps U_{lim} = 22,450 fps Stagnation Enthalpy = 2.5 x 10^8 ft^2/sec^2 s/r = 36.9 Re_∞/ft = 0.09 x 10^6
High Performance Shock Tube Fig. 1b (Achieved)	p_4 = 44,000 psia T_4 = 800°K Nitrogen, Helium	p_5 = 32,000 psia	———	———	———
Conventional High Performance Shock Tunnel, Mode 1 Figs. 1c and 11 (Predicted)	p_4 = 50,000 psia T_4 = 800°K Nitrogen, Helium	p_5 = 30,000 to 35,000 psia M_S = 2 to 6 (Tailored Interface)	———	———	M_∞ = 6 to 14 (See Fig. 11)
High Performance MHD Facility, Mode 2 Figs. 1d and 12 (Predicted)	p_4 = 37,000 psia T_4 = 700°K Helium	p_5 = 22,000 psia T_5 = 5000°K M_S = 8.0 (Overtailored Interface)	0	$\bar{U}_1$ = 10,100 fps $\bar{M}_1$ = 3.1 $\bar{U}_{11}$ = 10,750 fps $\bar{M}_{11}$ = 3.7 M_i = 4.3	M_∞ = 10 U_∞ = 12,000 fps U_{lim} = 12,800 fps $H_0 = 8.2 \times 10^7$ ft^2/sec^2 s/r = 29.8 Re_∞/ft = 0.56 x 10^6
			7	$\bar{U}_{10}$ = 16,100 fps $\bar{M}_{10}$ = 4.0 M_i = 4.5	Density Altitude = 142,000 ft M_∞ = 10 U_∞ = 18,650 fps U_{lim} = 19,700 fps Stagnation Enthalpy = 1.9 x 10^8 ft^2/sec^2 s/r = 33.9 Re_∞/ft = 0.12 x 10^6 T_∞ = 778°K

and the interim second-stage nozzle geometries are shown in Figs. 2 and 3. The first-stage nozzle has a square cross section and a 1°26′ divergence angle. Downstream of the accelerator section the nozzle is fabricated from fiberglass, and upstream the nozzle material consists of 10-in.-length Alumina inserts bonded to a fiberglass shell. The accelerator section consists of eleven pairs of beryllium-copper electrodes separated by 0.357-in.-thick nylon insulators. The nozzle (accelerator) sidewalls are frabricated from Lexan.® The accelerator is contained in a fiberglass shell and encased in a nonmagnetic steel alloy (Inconel®) pressure vessel. Without MHD operation, a solid copper channel can be used in the initial 34 in. of the nozzle.

Pertinent dimensions of the interim second-stage conical nozzle are the 20° half-angle, the 2-in.-inlet-diam, and a 12-in.-exit-diam (Fig. 2).

2.3 Electric and Magnetic Field Systems

A capacitive energy supply rated at 0.25 Mjoules is used to provide an electric field for the MHD accelerator operation with the standare driver. The supply consists of 190 capacitors each with a capacitance of 28μf and rated for 10,000 v. Each electrode pair has a simulated transmission line which consists of capacitors and inductors connected so that approximately constant voltage and current ($\pm$5%) are applied for 1 msec to the load, which is the conducting gas in the nozzle accelerator.

The magnetic (B) field source, Fig. 2, is a copper-wound aircore magnet designed for a field strength of 10 webers/m^2 (Ref. 9). The energy to power the magnetic coil is supplied by four homopolar generators (AEDC-VKF Tunnel F power supply,[9] which can deliver a maximum of 10^6 amp at 90 v. A field strength of 10 webers/m^2 requires 300,000 amp (150,000 amp for each coil half). Present and future operation has been limited to a maximum of 7.5 webers/m^2 in order not to exceed a maximum coil temperature of $\approx$200°F and to avoid possible structural degradation. The field strength has been determined

experimentally to be constant within $\pm 5\%$ over the length and width of the MHD accelerator.

2.4 Instrumentation

Piezoelectric transducers are used to measure the shock tunnel reservoir pressure on the top and bottom surface of the shock tube about $\frac{1}{2}$ in. from the end wall. Estimated accuracy of the systems is about $\pm 5\%$. Shock speed is measured using ionization or thin-film gages in conjunction with a raster oscilloscope and time-mark generator. Model pressures are measured using piezoelectric transducers having an estimated accuracy (including transducer and system error) of about $\pm 10\%$.

3. Demonstrated Performance Characteristics with MHD Augmentation

Application of MHD augmentation to increase the performance of aerodynamic test facilities has the primary advantage of adding energy directly to a moving stream; therefore, the equivalent reservoir conditions that would be required for a similar isentropic equilibrium expansion process are not required. This makes possible the attainment of test section conditions with equivalent reservoir pressures and temperatures far above the limits established by material capabilities in more conventional facilities. A second advantage is that the major portion of the energy can be added as direct kinetic energy, rather than thermal, so that the resulting gas stream is at a higher pressure than would be obtained if all the energy were added as thermal energy, such as by arc heating in a closed-volume reservoir.

The performance capabilities achieved using MHD augmentation are summarized in Table 1. Selected results which illustrate the accelerator gas dynamic performance characteristics and the flowfield quality are presented in this section. It seems appropriate to mention that over 500 firings of the Tunnel J facility (Fig. 1a) using MHD flow augmentation have been made. A summary of the nominal bank and electrode voltages and currents and magnetic field levels for these conditions is given in Table 2.

Table 2

	Power level – 1 (nominal)	Power level – 2 (nominal)
(Bank), V_0	$\approx$3000–5500 v	$\approx$3000–7500
(Electrode), V	$\approx$1000–1200 v	$\approx$1000–1500
(Electrode), I	$\approx$1500–2000 amp	$\approx$1500–3000
Load factor $V/\bar{U}Bh$	3.5–1	2–1
B	4 webers/m^2	5 webers/m^2
Energy stored in capacitors	29 Mjoules	57 Mjoules
Energy delivered to electrodes	19.5 Mjoules	32 Mjoules

3.1 Reservoir Conditions

For MHD operations, using hydrogen driving air, the shock Mach number (M_s) was about 8 which provided a near "tailored"[10] condition with a fairly uniform reservoir pressure lasting for about 1.0 msec; e.g., see Ref. 8. Shock tube performance data and run time studies have been reported in Refs. 8 and 11, respectively. The shock tunnel geometry is shown in Figs. 1a, 2, and 3; and the nominal test conditions are listed in Table 1.

3.2 Seed Distribution and Gas Conductivity Measurements

Sufficient levels and duration of gas conductivity are required for MHD operation.[1,3,4,5,12] Conductivity levels and duration have been measured in the Tunnel J MHD nozzle accelerator (Figs. 2 and 3) using the induced voltage generated by the conducting gas passing through the magnetic field and with a broadside microwave technique. These experimental measurements have shown that the duration of gas conductivity is about 3 msec. Discharge time of the MHD accelerator is 1 msec.

A seeder mechanism is located 5 in. from the shock tube end wall as illustrated in Fig. 2. Calibration of the anhydrous potassium carbonate (K_2CO_3) seed mass ratio injected into the gas and gas electrical resistance experiments has established that 1 gm of seed provided sufficient gas conductivity for MHD operation. Assuming homogeneous distribution occurs, 1 gm of seed (0.7 gm injected) gives a mass fraction (seed/air) of $\approx 1.3\%$.

3.3 First-Stage Nozzle Performance and Flow Calibration

Without MHD augmentation, sidewall static pressures have been measured at four locations in the first-stage nozzle and on centerline at the nozzle exit using static-pressure flat-plate and cone-cylinder probes. Experimental data are presented and compared with AEDC-VKF¶ and Cornell[13] theoretical nonequilibrium and equilibrium solutions (with and without viscous losses) in Fig. 3. As indicated by the data spread, the results show that with good design, fabrication, and assembly techniques pressure, distributions that are comparable in quality to the all-copper channel (see Sec. 2.2) can be obtained using the MHD-segmented accelerator and insulator sections. Comparison of the experimental data with the Cornell theory[13] indicates that the flow is in or very near a state of thermochemical equilibrium. The spread of the static-pressure data obtained from several runs with MHD augmentation (Power Level – 1) is also shown in Fig. 3. With MHD energy addition, the static pressure experiences a 90% rise which is in good agreement with the one-dimensional AEDC-VKF MHD computer program¶ results. Typical oscilloscope traces of the sidewall static pressure are presented in Fig. 4.

Figure 4 compares the first-stage nozzle exit centerline powered and unpowered (UNP) pitot-pressure ratios to the calculated values.¶ The $(p_o')_{UNP}$ value was inferred from the measured ratios obtained using the segmented MHD channel ($p_{o'UNP}/p_5 = 0.030$). Typical pitot-pressure oscilloscope traces measured at the exit of the first stage ($x = 61$ in.) are also shown in Fig. 4 for an unpowered and the two-powered conditions. The effect of MHD augmentation is evident, with essentially a step function lasting

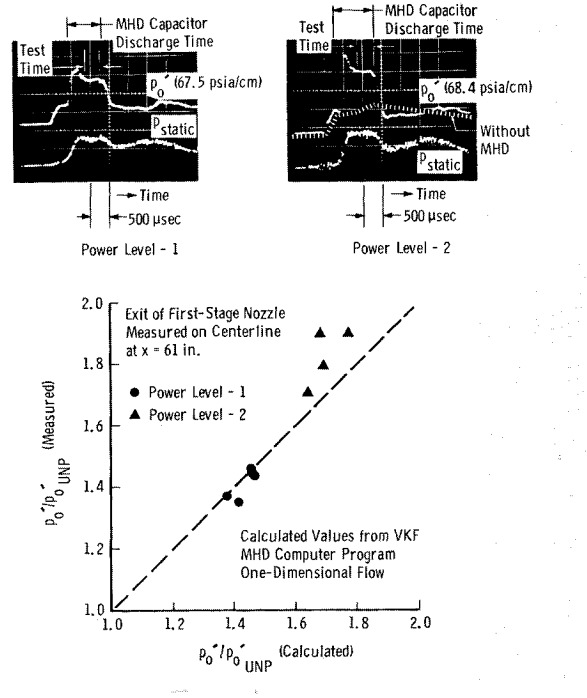

Fig. 4 Measured pitot-pressure ratio vs calculated values, with MHD augmentation.

¶ W. S. Norman was primarily responsible for the analytical solutions and development of the computer program.

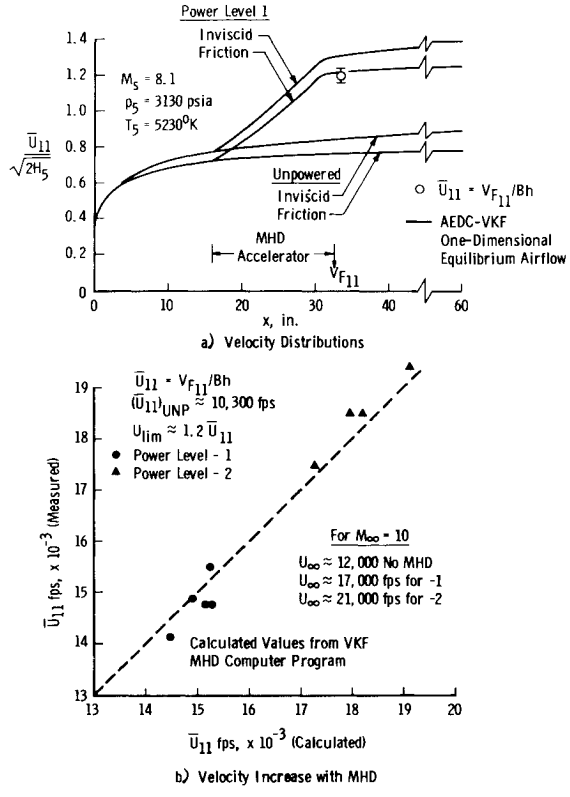

Fig. 5 Measured velocity vs calculated values, with MHD augmentation.

approximately 1 msec being imposed on the pitot pressure. There is a second starting wave process which lasts approximately 0.5 msec when the MHD accelerator fires, as indicated on the oscilloscope traces presented in Fig. 4. The steady-state test time of 0.5 msec is also indicated.

Calculated axial velocity distributions in the MHD accelerator channel obtained using the VKF viscous flow computer program¶ have been compared with the experimentally determined flow velocities obtained without MHD. The Winkler and Cha total turbulent boundary-layer skin-friction law[14] was used to estimate viscous losses. A value of the total skin-friction coefficient of $C_f = 0.0028$ at the accelerator exit provided agreement within $\pm 6\%$ between the measured velocities inferred from $\bar{U} = V_F/Bh$ and theory. Experimental results from several runs using a deteriorating "rough" wall, fiberglass insulator section upstream of the MHD accelerator produced a 10% decrease in the measured velocities. The influence of seed (K_2CO_3) on the velocity distribution was not discernible above the run-to-run data scatter. These nozzle flow velocity measurements made without MHD augmentation have established that a mean flow velocity can be determined using the induced voltage measurements from the eleven electrodes, the measured magnetic field strength, and the physical law $V_F = B\bar{U}h$. This verification is necessary since electrode No. 11 is used to establish the accelerated flow velocity with MHD augmentation.

Velocity distributions in the first-stage nozzle, with and without MHD augmentation, calculated using the AEDC-VKF computer program are shown in Fig. 5a. The increase in flow velocity obtained with power level − 1 condition and determined experimentally using the inferred velocity from number eleven electrode voltage (V_F) is seen to be in good agreement with the one-dimensional MHD theory¶ with viscous losses. A summary of the experimental mean-flow velocity data obtained with MHD augmentation for power levels − 1 and − 2 is compared with the theoretical predictions¶ in Fig. 5b, and good agreement is seen to exit. Without MHD augmentation, the nominal theoretical velocity at electrode number eleven was 10,300 fps. Increases in flow velocity of about 40% and 80% obtained using power levels − 1 and − 2, respectively, are to be noted. The run-to-run repeatability is illustrated by the data scatter. Also note that for a Mach number of ten in the second-stage nozzle, the nominal freestream velocities for $M_\infty = 10$ were 17,000 and 21,000 fps and the limiting velocities ($M_\infty \to \infty$) were 19,000 and 22,500 fps for power level − 1 and − 2, respectively.

The measured induced voltage ($V_F = \bar{U}Bh$) can be used to infer a mean-flow velocity as discussed in the above paragraphs. Pitot-pressure measurements on the other hand are directly related to local values of velocity. It can be shown that for one-dimensional hypersonic flow

$$(p_o')\ \text{powered}/(p_o')\ \text{unpowered} \approx (U)\ \text{powered}/(U)\ \text{unpowered}$$

This relationship is verified in Fig. 10c of Ref. 8. Therefore, the pitot-pressure measurements and the induced voltage measurements provide two independent measurements for evaluating flow velocity increases resulting from MHD augmentation.

The increased kinetic energy of the airstream is computed to be equivalent to a power input of 16.4 and 28.4 Mw for the power level − 1 and − 2 conditions, respectively. Measurements of electrode current and voltage during the 1-msec accelerator discharge time show the power supplied to the accelerator from the capacitor banks to be 19.5 and 32.0 Mw for the respective operating conditions. Thus, 85%–90% of the power transmitted to the electrodes is converted into kinetic energy. This high efficiency may result from the fact that the boundary layer in the accelerator channel is turbulent. Data presented in Ref. 12 show that for freestream conditions of 10 atm pressure, temperature of 3500°K, and current density of the order of 100 amps/cm^2, the voltage drop through a laminar boundary layer is approximately 50 times that for a turbulent boundary layer. These conditions are of the same order as those found in the Tunnel J MHD accelerator for both operating conditions. Thus, a similarly small (turbulent boundary layer) voltage drop might be expected, which may be one factor in the observed highly efficient utilization of the power applied to the accelerator.

3.4 Second-Stage Interim Nozzle Calibrations

The inlet to the second-stage nozzle is smaller than the accelerator first-stage nozzle exit and thus performs the dual

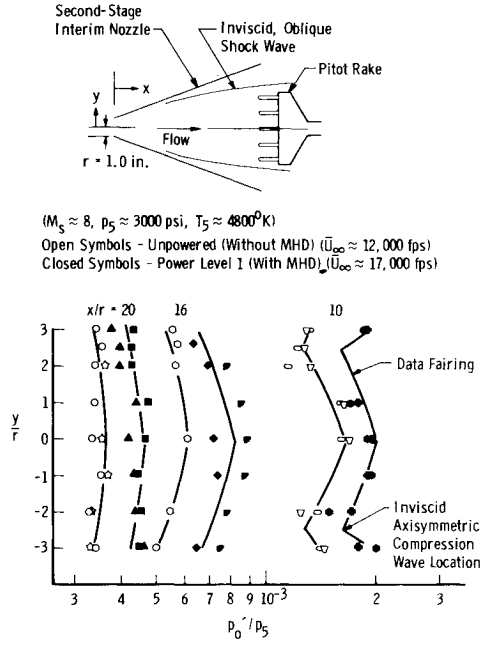

Fig. 6 Pitot-pressure profiles measured in second-stage nozzle, with and without MHD augmentation.

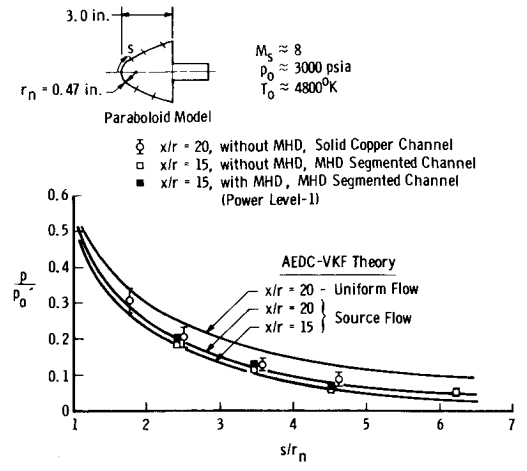

Fig. 7 Pressure distribution on a paraboloid model, with and without MHD augmentation.

purpose of dumping a portion of the accelerator channel viscous boundary-layer flow and also allows a small test section diameter for a given hypersonic Mach number (Fig. 2). Analytical studies of a supersonic flowfield entering a conical nozzle of this type have demonstrated the existence of a compression system which coalesces into an oblique shock wave embedded in the flowfield, as illustrated in Fig. 6. This compression arises because of the axisymmetric nature of the flow. Pitot-pressure surveys conducted in the 20° nozzle have established the existence of this shock wave and confirmed its location to be near the predicted locations.

Pitot-pressure profiles (with and without MHD augmentation) measured at several axial locations are presented in Fig. 6. The uniformity of the increase in pitot pressures both radially and axially realized using MHD augmentation is to be noted. Also, the profiles obtained using MHD have the same shape as the unpowered data; and the data quality as defined by the data scatter obtained using MHD is about the same as the unpowered data. The MHD data were obtained at power level −1 ($U_\infty \approx 17{,}000$ fps). The curvature of the profiles shown in Fig. 6 is a direct result of the source-like nature of the nozzle flow and the nonuniformity of the flow at the nozzle inlet; e.g., see Ref. 8.

In addition to the pitot-pressure profile measurements at discrete locations, extensive measurements of the nozzle centerline static and pitot pressure without MHD augmentation have been made for the entire nozzle length; e.g., see Fig. 12 in Ref. 8. These nozzle centerline measurements have identified a weak (isentropic) shock wave system which forms on the fairly thick (0.020-in.) leading edge of the inlet and spills into the nozzle. Assuming isentropic flow and using the measured pitot-pressure distribution in conjunction with the inlet conditions, centerline Mach number distribution in the second-stage nozzle can be computed. Results of such calculations assuming frozen chemistry and frozen vibrational energy and also equilibrium flow are presented in Fig. 12 of Ref. 8. Calculations have indicated that the second-stage nozzle flow for the 20° angle expansion will be frozen very near the inlet of the second-stage nozzle.

4. Demonstrated Aerodynamic Measurements Using MHD

Surface pressure measurements on a paraboloid model with and without MHD augmentation and nondimensionalized by the stagnation point pressure on the nose of the model are shown in Fig. 7. Calculated distributions are also shown, both for the case of a uniform freestream and also with corrections for source-flow effects which were obtained from an analysis using the measured centerline pitot-pressure gradient (Fig. 6). Good agreement between the experimental data and theory is seen to exist. A limited amount of static-pressure measurements on a 30° half-angle sharp cone and heat-transfer-rate distributions on hemisphere probes with and without MHD augmentation also have been made, and selected data have been presented in Ref. 8.

The experimental data and theoretical results presented in Figs. 3–7 have demonstrated the validity of the two-stage nozzle concept and have shown that quantitative nozzle flow calibrations and pressure distributions on test models can be obtained in an MHD-augmented impulse facility.

The presence of seed (see Sec 3.2) can contribute to flowfield particle contamination as well as potentially affecting the heat-transfer-rate measurements in high enthalpy equilibrium or nonequilibrium chemically reacting flows. Stagnation heat-transfer-rate measurements on hemisphere-cylinder calibration probes with and without seed material in the flow but without MHD augmentation have not shown any measurable effects of the K_2CO_3 seed material. However, much work remains to be done to establish the effects of seed on heat-transfer-rate measurements in chemically reacting flow.

5. Demonstrated Capability of the High Performance Driver

5.1 Driver Performance

Performance characteristics of the high performance driver have been defined in static heating calibration tests[8] using helium and nitrogen as the driver gases at gas pressures and bulk temperatures up to 44,000 psia and 800°K, respectively. During these tests, the heater element reached a maximum (top surface) temperature of ≈ 1400°F (1050°K) with the minimum (bottom surface) temperature having a corresponding maximum value of ≈1100°F (810°K). The maximum measured circumferential gradient in the element temperature and the vertical gradient in the gas temperature were about 25% (in absolute temperature); e.g., see Ref. 8. The large heat-transfer rates encountered from the convective currents at high densities necessitated the use of an eccentric heating element so as to counterbalance the convective heat transfer with reduced resistance heating at the top and increased resistance heating at the bottom.

The driver pressure vessel was designed to accommodate a heating cycle of 3 min. The heater element power supply is rated for a current of 60,000 amp at 120 v. Temperature measurements on the pressure vessel inner wall have verified

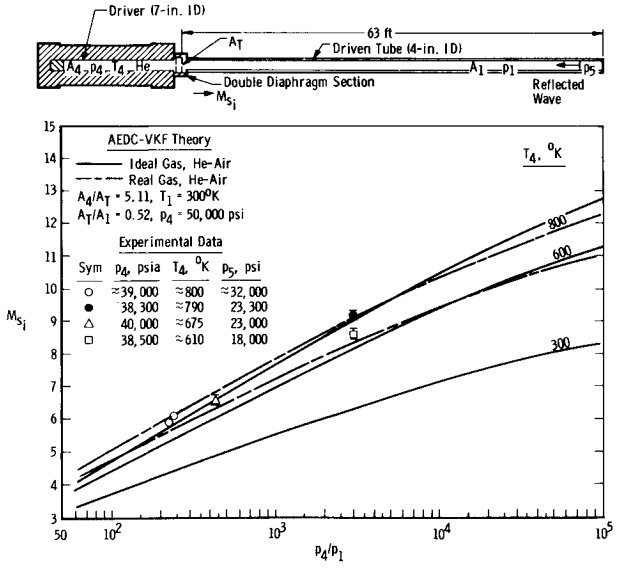

Fig. 8 Tunnel J shock tube performance using high performance driver (Helium driving air).

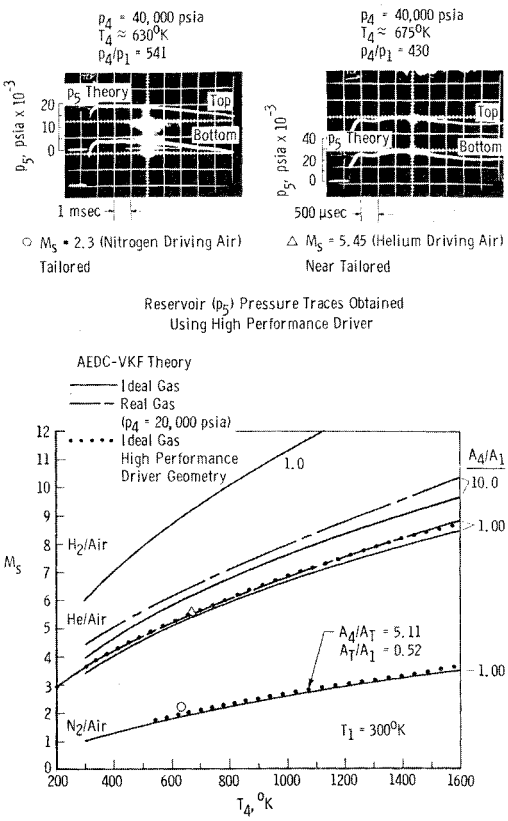

Fig. 9 Shock tunnel interface tailoring conditions.

the analytical estimates. Extensive calibration data have shown that a normal heating cycle time of 3 min is adequate to produce the maximum design driver conditions (p_4 = 50,000 psi, T_4 = 800°K).

5.2 Shock Tube Performance

Experimental and theoretical¶ shock tube performance results obtained using the high performance driver with helium driving air are shown in Fig. 8. The good agreement between experimental data and theory is to be noted. Experimentally measured shock wave attenuations for M_s = 8.2 and 5.5 have shown that a decrease in shock speed from 10%–20% occurred over the driven tube distance (l_1 = 63 ft), respectively. Experimental data have also been obtained using nitrogen driving air; e.g., see Fig. 17c, Ref. 8.

Figure 9 presents theoretical¶ results showing the shock tube driver temperatures and shock Mach number required to provide interface tailoring for several driver-driven tube geometries. The strong effects of driver gas composition, driver gas temperature and moderate effects of diameter ratios and real gas are evident. Two reservoir pressure oscilloscope traces obtained at M_s = 2.3 (nitrogen driving air) and at M_s = 5.45 (helium driving air) are included in Fig. 9 and provide verification that interface tailoring can be obtained and confirm that the theoretical results are applicable.

The wave diagram presented in Fig. 10 is for the M_s = 8.0 MHD condition and is one of the three test conditions considered to be of primary aerodynamic interest as will be discussed in Sec. 6.2. The M_s = 8 condition will be required for MHD operation since it is anticipated that a reservoir temperature near about 5000°K in conjunction with about 1% mass ratio of K_2CO_3 seed will be required to provide sufficient gas electrical conductivity levels. The interface is not tailored at this M_s and T_4 values as can be determined from the p_5 oscilloscope trace included in Fig. 10. The theoretically predicted values of p_5 included in Fig. 10 indicate that the interface would be overtailored.

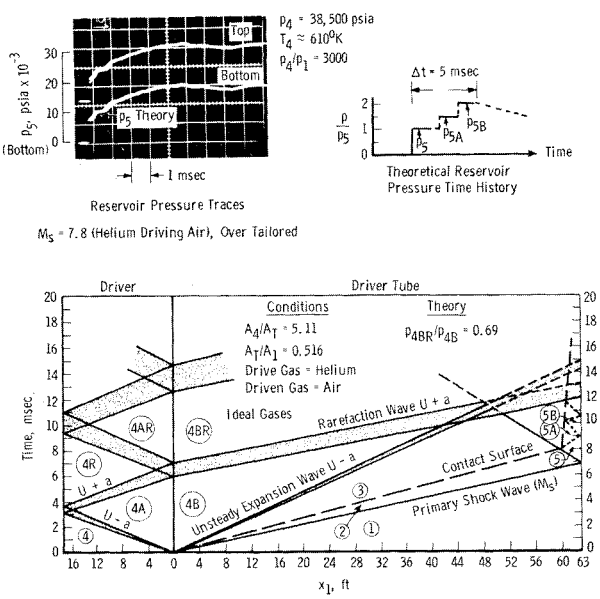

Fig. 10 Reservoir pressure history and theoretical wave diagram using high performance driver, MHD condition (M_s = 8, T_4 = 800°K, over tailored).

6. Recent Facility Modifications and Predicted Capabilities

Recent modifications to the Tunnel J facility have included 1) addition of a conventional 5°, half-angle nozzle and test section (Mode 1), Figs. 1c and 11a; 2) addition of a new second-stage

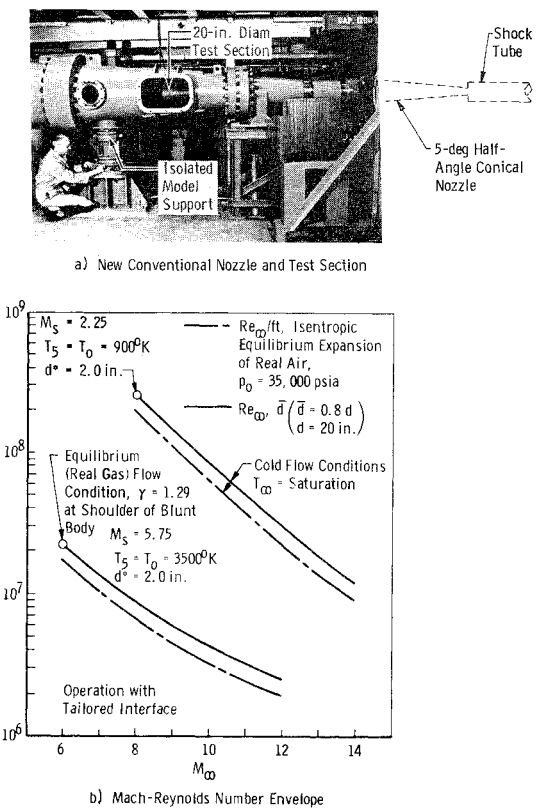

Fig. 11 Predicted performance capability of modified Tunnel J with conventional shock tunnel nozzle (Mode 1).

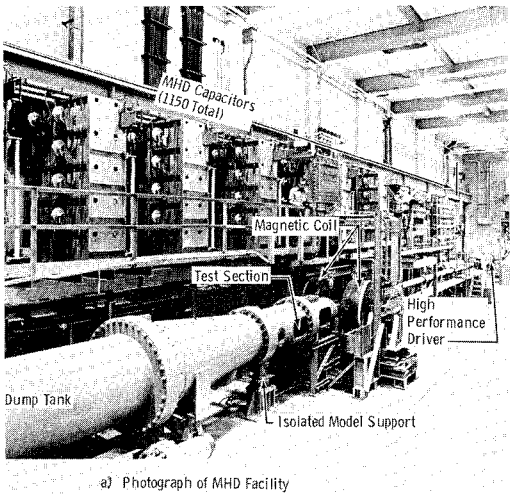

a) Photograph of MHD Facility

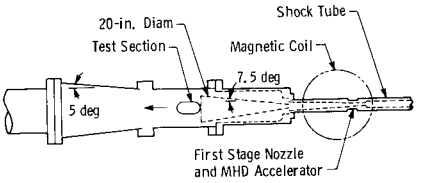

b) Sketch Illustrations First and Second State Nozzles and Test Section

Fig. 12 Modified high performance MHD shock tunnel (J) with new test section (Mode 2).

nozzle and test section for MHD operation (Mode 2), Figs. 1d and 12; 3) new isolated model support common to both Modes 1 and 2, Fig. 11a; and 4) the addition of 950 MHD capacitors, Fig. 12. These modifications will enable aerodynamic testing to be conducted in a conventional shock tunnel having high enthalpy, very high Reynolds numbers, and equilibrium flows (Mode 1), and in the MHD-augmented facility having nonequilibrium flow with freestream velocities near 20,000 fps (Mode 2).

The modified Tunnel J facility provides the capability for a single facility to provide a wide range of test conditions not available in other existing facilities. The capability to make measurements on the same model, using the same instrumentation, mounted on the same model support system in an equivalent size test section (20-in.-diam) will provide a significant and major ground testing capability by allowing experimental results obtained in high enthalpy equilibrium and nonequilibrium flow environments to be compared directly to "ideal-gas" experimental data. This section provides detailed information on Modes 1 and 2. A summary of the predicted test conditions for Modes 1 and 2 is presented in Table 1.

6.1 High Reynolds Number Shock Tunnel Facility (Mode 1)

For this mode of operation, a 5°, half-angle conical nozzle will be used with the high performance driver, Figs. 1c and 11a. Results presented in Figs. 8 and 9 have established that a reservoir pressure (p_5) of approximately 30,000 to 35,000 psi can be obtained using the full-scale impulse-heated driver operating at a gas pressure and temperature of 50,000 psi and 800°K, respectively, and with interface tailoring for $2.3 \lessapprox M_s \lessapprox 6.0$. The Tunnel J Mach number range and corresponding maximum Reynolds numbers for isentropic equilibrium expansions of air to the theoretical saturation point are shown in Fig. 11b.

In addition to providing high Reynolds number capabilities at hypersonic conditions, Mode 1 will also have the unique capability of providing a real-gas equilibrium test environment on blunt-nose models having a natural, fully developed turbulent boundary layer. Blunt bodies and geometries with deflected flaps, etc., are the geometries most likely to experience significant real-gas effects. Calculations show that reservoir conditions of $T_o = 3500$°K and $p_o = p_5 = 35{,}000$ psi and $M_\infty = 6$ are sufficient to produce a temperature of 1700°K at the model shoulder with $\gamma = \gamma_E = 1.29$, which defines an equilibrium real gas. The Reynolds number and Mach number ranges for the $T_o = 3500$°K test condition ($M_s = 5.75$) are included in Fig. 11b.

The measured steady-state time of the reservoir pressure for the $M_s = 5.75$ condition ($T_o = 3500$°K) was about 3 msec, as shown in Fig. 9. For the $M_s = 2.25$ test condition ($T_o = 900$°K), the measured steady-state reservoir pressure was about 4 msec as indicated in Fig. 9.

Using the method of Ref. 15, the end of boundary-layer transition on a 10° half-angle sharp cone is estimated to occur at $x_t \leqq 5$ in. for the $M_\infty = 6$, $Re_\infty/\text{ft} = 20 \times 10^6$ (real gas, $\gamma = 1.29$) test condition. For the high Reynolds number ideal-gas test condition, $M_\infty = 8$, $Re_\infty/\text{ft} = 200 \times 10^6$, an $x_t \leqq 1.0$ in. location is predicted.

6.2 MHD-Augmented Facility (Mode 2)

Future MHD testing will be with the high performance driver and a new 7.5°, half-angle second-stage nozzle with a 20-in.-diam test section (Figs. 1d and 12). Structural limitations will restrict operation of the modified MHD facility to a maximum reservoir pressure of 22,000 psi. An additional capacitive power supply consisting of 950 capacitors rated for 3000 v at 125 μf each is being added to supply extra energy. The total energy supply will increase from 0.25 to 0.75 Mjoules. These modifications will increase the discharge time from 1 to 3 msec.

The theoretical wave diagrams in the shock tube, with a typical oscilloscope trace of the reservoir pressure (p_5) obtained using the high performance driver was presented in Fig. 10 and discussed. For future MHD test conditions, the nozzle quasi-steady-state flow time is estimated to be 4.6 msec. The modified MHD E-field discharge time of 3 msec will provide a near steady-state accelerated flow time of about 2.4 msec. Computer MHD accelerator performance characteristics for a reservoir pressure of 22,000 psi using the existing eleven-electride accelerator, the existing magnetic coil at a B-field strength of 7 webers/m^2, and a modified E-field have predicted that a freestream velocity of about 18,650 fps at $Re_\infty/\text{ft} = 0.12 \times 10^6$ (density altitude of 142,000 ft) at $M_\infty = 10$ can be achieved. A summary of the predicted performance is presented in Table 1.

7. Freestream Gas Compositions for Modes 1 and 2

The desired thermochemical state of the test gas for conducting hypervelocity aerothermodynamic testing is for the freestream test gas to be essentially an air composition with $\gamma \approx 1.4$. This requirement dictates that the hypersonic nozzle expansion process occur in or near a state of equilibrium and that chemical freezing occur relatively late in the expansion process. Harris[16] has shown that nonequilibrium effects in the expansion of high enthalpy air could be correlated as a function of reservoir entropy. Ring and Johnson[17] made extensions to the entropy correlation concept. A reservoir entropy of $S/R = 32$ has been specified as the approximately upper limit that chemical equilibrium can be maintained in the hypersonic expansion of air.[16,17]

For the Mode 1 conventional shock tunnel operation, a maximum value of $S/R = 26.3$ will occur at the $p_o = 35{,}000$ psi, $T_o = 3500$°K test condition. This value of S/R is well below the criteria of $S/R = 32$ defined in Refs. 16 and 17 to be necessary for an equilibrium expansion to occur with an air composition and $\gamma_\infty = 1.4$ existing in the test section freestream.

For Mode 2, it is assumed the flow leaving the first-stage nozzle is in equilibrium (see Fig. 3). The gas expansion process and gas composition has been computed using Ref. 13 with the assumption that at the inlet of the second-stage nozzle

the gas is in a state of chemical nonequilibrium and vibrational equilibrium. The mass fractions of the gas composition at a test section condition of $M_\infty = 10$, $T_\infty = 778°K$, $p_\infty = 0.083$ psi were calculated to be $N_2 = 0.726$, $O_2 = 0.145$, $O = 0.0534$, $NO = 0.0618$, $AR = 0.0126$ with $S/R = 33.9$ and $\gamma_\infty = 1.41$. It should be noted that these computations are not inconsistent with the maximum value of $S/R = 32$ stated in Refs. 16 and 17 to be required for an equilibrium expansion of air to occur.

8. Summary and Concluding Remarks

Extensive experimental and theoretical investigations conducted in support of the development of a ground test facility capable of simulating high enthalpy thermochemical equilibrium and nonequilibrium, high-density hypervelocity flows with extended ranges of Mach number-Reynolds number have been conducted in the Arnold Engineering Development Center, von Kármán Gas Dynamics Facility. The following conclusions are based on extensive experimental data obtained in the AEDC-VKF Tunnel J facility and on predicted capabilities of the recently modified Tunnel J facility (Modes 1 and 2).

1) Successful progress toward the development of an MHD-augmented shock tunnel (J) has been dependent on four major accomplishments: development of a full-scale, high performance, impulse-heated shock tube/tunnel driver; development of an MHD-augmented nozzle accelerator suitable for conducting aerodynamic tests; definition and calibration of the flow process in a two-stage nozzle system; and development of model instrumentation that would function in an MHD-augmented flow environment.

2) Experimental data obtained in the shock tunnel (J) have verified the validity and applicability of a shock tunnel employing an MHD nozzle accelerator for providing large increases in flow velocity. A maximum increase in test section flow velocity from 12,000 fps to 21,000 fps at $M_\infty = 10$ has been demonstrated. Good agreement between experimental data and one-dimensional MHD theory has been shown. Extensive operational experience, detailed calibration data, and basic aerodynamic measurements (model surface pressures) have been successfully obtained using the MHD nozzle accelerator.

3) Development of a full-scale (21-ft length by 7.0-in. i.d.), internal resistance, impulse-heated, high performance shock tube/tunnel driver has been successfully completed. Driver and shock tube performance characteristics have been experimentally established using helium and nitrogen driver gases at pressure (p_4) up to 44,000 psi at gas temperatures (T_4) up to 800°K.

4) When operated as a conventional high performance shock tunnel (with a tailored interface) "ideal-gas" test conditions over a Mach number range from 8 to 14 with Reynolds numbers (based on a test section diameter of 20 in.) up to 250×10^6 and 15×10^6, respectively, are predicted for the modified Tunnel J facility (Mode 1).

5) When operated as a conventional shock tunnel (Mode 1) with $p_o = 35{,}000$ psi and $T_o = 3500°K$ (tailored interface), an equilibrium flow "real-gas" ($\gamma = 1.29$) local test condition is predicted on blunt bodies having fully developed turbulent flows with length Reynolds numbers of about 25×10^6 at $M_\infty = 6$. This will be a useful test condition for experimentally studying model base pressures and model flap pressures and heat-transfer rates when exposed to high enthalpy, equilibrium turbulent boundary-layer flows.

6) When operating as a high performance, MHD-augmented shock tunnel, while maintaining a freestream near air gas composition with $\gamma = 1.41$, flow velocities up to about 19,000 fps at $M_\infty = 10$ (equivalent density altitude of 142,000 ft) are predicted for the modified facility (Mode 2).

References

[1] Ring, L. E., "General Consideration of MHD Acceleration for Aerodynamic Testing," Paper presented at the AGARD Specialists' Meeting "Arc Heaters and MHD Accelerators for Aerodynamic Purposes," Sept. 21–23, 1964, Rhode-Saint-Génèse, Belgium; also, AEDC-TR-64-256 (AD453419), Dec. 1964, Arnold Engineering Development Center, Arnold Air Force Station, Tenn.

[2] Norman, W., "One-Dimensional Magnetohydrodynamic Equations for a Non-Ideal Gas with Application to Single Ionized Argon," AEDC-TR-65-185 (AD470771), Sept. 1965, Arnold Engineering Development Center, Arnold Air Force Station, Tenn.

[3] Norman, W. and Chmielewski, G. E., "Limit Duplication Lines for Isothermal, Constant Loading Factor, J × B Accelerators," AEDC-TR-65-37, Feb. 1965, Arnold Engineering Development Center, Arnold Air Force Station, Tenn.

[4] Warren, W. R., Harris, C. J. et al., "Feasibility Study of a High Density Shock Tunnel Augmentation by a Magnetohydrodynamic Accelerator," AEDC-TR-65-225 (AD472465), Oct. 1965, Arnold Engineering Development Center, Arnold Air Force Station, Tenn.

[5] Grabowsky, W. R., Durran, D. A., and Mirels, H., "Performance of a 500-K joule MHD Wind Tunnel," *AIAA Journal*, Vol. 7, No. 10, Oct. 1969, pp. 1846–1852.

[6] Leonard, R. L. and Rose, P. H., "Feasibility of a High-Performance Aerodynamic Test Facility," *AIAA Journal*, Vol. 6, No. 3, March 1968, pp. 448–457.

[7] Warren, W. R. and Harris, C. J., "A Critique of High Performance Shock Tube Driving Techniques," *Proceedings of the Seventh International Shock Tube Symposium*, University of Toronto Press, Toronto, Ontario, Canada, 1969.

[8] Pate, S. R., Siler, L. G., Stallings, D. W., and Wagner, D. A., "Development of the AEDC-VKF Tunnel J—A Real Gas High Density, True Velocity, Hypersonic, Aerodynamic Test Facility," AIAA Paper 72-993, Palo Alto, Calif., 1972.

[9] Patterson, J. N., "Inductive Power Supply for a 100-in. Hotshot Wind Tunnel," AEDC-TR-66-260, March 1967, Arnold Engineering Development Center, Arnold Air Force Station, Tenn.

[10] Wittliff, C. E., Wilson, M. R., and Hertzberg, A., "The Tailored Interface Shock Tunnel," *Journal of the Aeronautical Sciences*, Vol. 26, No. 1, April 1959, pp. 219–228.

[11] Lacey, J. J., Jr., "Experimental Shock Tube Test Time—Turbulent Regime," *Proceedings of the Seventh International Shock Tube Symposium, June 23–25, 1969*, edited by I. I. Glass, University of Toronto Press, Toronto, Ontario, Canada, 1970.

[12] Goins, E. E. and Norman, W., "Studies of Electrical Characteristics of Gasdynamic Boundary Layers in Seeded Diatomic Gases," AEDC-TR-68-111, June 1968, Arnold Engineering Development Center, Arnold Air Force Station, Tenn.

[13] Lordi, J. A., Mates, R. E., and Mosell, J. R., "Computer Program for the Numerical Solution of Nonequilibrium Expansions of Reacting Gas Mixtures," CAL Rept. AD-1689-A-6, Oct. 1965, Cornell Aeronautical Lab., Buffalo, N.Y.

[14] Winkler, E. M. and Cha, M. H., "Investigation of Flate Plate Hypersonic Turbulent Boundary Layers with Heat Transfer at a Mach Number of 5.2," NAVORD Rept. 6631, Sept. 15, 1959, Naval Ordanance Lab., White Oak-Silver Spring, Md.

[15] Pate, S. R., "Measurements and Corrections of Transition Reynolds Numbers on Sharp Slender Cones at High Speeds," *AIAA Journal*, Vol. 9, No. 6, June 1971, pp. 1082–1090.

[16] Harris, C. J., "Comment on Nonequilibrium Effects on High Enthalpy Expansion of Air," *AIAA Journal*, Vol. 4, No. 6, June 1966, pp. 1148–1149.

[17] Ring, L. E. and Johnson, P. W., "Correlation and Prediction of Air Equilibrium in Nozzles," AIAA Paper 68-378, San Francisco, Calif., 1968.